A prototype low-carbon segmented concrete shell building floor system

Robin Oval[a], Mishael Nuh[a], Eduardo Costa[b], Omar Abo Madyan[c], John Orr[a,*], Paul Shepherd[b]

[a]*Structures Research Group, Department of Engineering, University of Cambridge, Cambridge, United Kingdom*
[b]*Department of Architecture and Civil Engineering, University of Bath, Bath, United Kingdom*
[c]*Centre for Smart Infrastructure and Construction, Department of Engineering, University of Cambridge, Cambridge, United Kingdom*

Abstract

Concrete shell structures offer a mechanically efficient solution as a building floor system to reduce the environmental impact of our buildings. Although the curved geometry of shells can be an obstacle to their fabrication and implementation, digital fabrication and affordable robotics provide a means for the automation of their construction in a sustainable manner at an industrial scale. The applicability of such structures is demonstrated in this paper with the realisation of a large-scale concrete shell floor system, completed by columns, tie rods, and a levelled floor. The shell was prefabricated off-site in segments that can be transported and assembled on-site, and which can be disassembled to enable a circular economy of construction. This paper presents the conceptual and structural design; the automation of fabrication, thanks to an actuated, reconfigurable, reusable mould and a robotic concrete spraying process; the strategy and sequence of assembly and disassembly on-site using standard scaffold elements; and the sustainability assessment using life-cycle analysis. This prototype offers a reduction of about 50% of cradle-to-gate embodied carbon benchmarked against regular flat slabs before further improvement and optimisation.

Keywords: concrete structures, funicular shells, segmented shells, automated construction, flexible formwork, reconfigurable mould, concrete spraying, robotic fabrication, sustainability, life-cycle analysis, deconstruction.

1. Introduction

1.1. Context and literature review

The construction industry is responsible for nearly half of the carbon emissions of the UK [5], while cement production accounts for about 7% of the greenhouse emissions worldwide [4]. Building floors represent around 60% of the mass of a building, and have an impact on the design of the columns, walls and foundations [6, 26]. The potential structural efficiency of concrete is lost due to the fabrication process of concrete structural components, largely relying on timber boards as moulds into which concrete is poured. Such a requirement constrains designs to prismatic forms that are extremely different from the more efficient organic shapes. Building such complex shapes results in lower carbon content in the final structure, but potentially higher carbon impact and financial cost from the formwork material and labour, especially if the moulds can only be used once and produce waste [13, 33]. To reduce the carbon impact of the construction industry and achieve more sustainable structures, the design of efficient structural systems must take into consideration and integrate low-waste fabrication processes.

Flat slabs rely on bending to carry loads and, therefore, need structural thickness, and reinforcement in the case of concrete, resulting in a high embodied carbon. *Shells* rely on their membrane behaviour, thanks to their curvature and external thrust at the supports. Using the lower-bound theorem of plasticity theory

*Corresponding author
Email address: jjo33@cam.ac.uk (John Orr)

Figure 1: The OAK, ACORN's demonstrator of a segmented ribbed concrete shell as a building floor for a circular economy of construction ©John Orr.

to assess stability of masonry structures [28], designing a *funicular shape* for the primary load case using form finding and optimisation methods [3] yields a shell that experiences *compressive stresses* only. For secondary load cases, the shell may experience a degree of tension and bending, depending on the variability of load cases, which can be solved with reasonable thickening of the shell and/or the addition of tensile reinforcement. As such, a shell can be thinner than plates such as flat slabs and require less reinforcement.

Curved structures like shells are however more challenging to build. The fabrication of these structures can account for a large part of the embodied carbon, due to non-standard formwork [13], especially when milled foam blocks or tailored timber boards are used as moulds to cast concrete. Structures like gridshells [12, 58, 64], membranes [25] or cable nets [18, 51] can serve as *flexible formwork* for on-site casting of monolithic concrete structures. In these cases, the shape is controlled by the boundary conditions and the prestress in the formwork, which either stays in place, to potentially act as permanent reinforcement, or is removed for possible reuse. Reusing and reconfiguring such a mould to perform mass-customisation of the necessary accuracy is key to reducing the environmental impact of the construction of shell structures. *Off-site construction*, relying on *automation* and *robotics*, provides a suitable environment to achieve this. *Reconfigurable moulds* allow the production of curved concrete elements by casting on a flexible formwork, supported by a grid of pins that can move vertically to modify the shape of the mould [57]. Such moulds by Adapa [1] have already been successfully applied to the production of concrete shell elements bracing a steel frame for the roof of Kuwait International Airport [43].

Manufacturing concrete shells with the desired thickness is a challenge for traditional casting, especially if the shell has a variable thickness and integrates ribs for material economy and structural efficiency. To address this, additional formwork elements can act as guides for builders during on-site manufacturing. Elements like studs can inform the local target thickness, while also providing vertical spacing and shear reinforcement [18]. Lightweight blocks can mould ribs, whether these blocks are produced from plastic [42, 27, 9, 29], cut from foam [53, 16], or printed in concrete, foam or clay [38, 62], at the cost of a more elaborate, and potentially wasteful, fabrication process.

As opposed to pouring, other deposition strategies are more suitable for shells, especially with variable thickness, to cast and compact concrete on a curved surface without resorting to vibrating it, which would

alter the thickness distribution from the target. Geometrical accuracy during fabrication is important for concrete shells, whose buckling behaviour is sensitive to imperfections [54, 40]. Automation of such *additive fabrication processes* like robotic 3D printing [23, 11] or spraying [36, 63] of concrete provide the accuracy required to build complex concrete structures. Particularly, spraying provides the following benefits versus printing: higher speed in deposition; compaction; inclusion of fibre reinforcement; and absence of cold joints.

Scaffolding for on-site assembly of prefabricated elements presents similar challenges to formwork for on-site casting. The main objective is to avoid the use of custom scaffold elements to allow reuse, as well as to reduce the total amount of elements for efficiency, ideally assembling scaffold-free thanks to, for instance, informed structural segmentation [31, 49] or robot-aided construction [48, 41].

Beyond assembly, monolithic concrete structures are hard to disassemble, making them unaffordable for reuse in a *circular economy of construction* and leaving destruction as the sole alternative [56]. Structures must be designed for disassembly, reuse, and, eventually, reconfiguration to extend the life span of the structural components beyond that of the building. For such structures, a key aspect is the structural *segmentation*, which is already necessary for transport between the factory and the construction site, while joining the segments using *reversible dry connections*, which excludes on-site casting and grouting.

1.2. Problem statement and research objectives

Building structural concrete shells using off-site reconfigurable moulds and flexible formwork offers an interesting means to reduce the environmental impact of buildings, particularly floors. Nevertheless, there are many challenges related to this approach to construction. Structural shells, as opposed to cladding panels, must be thicker and offer a variable thickness to optimise material use, classically thinner at the centre and thicker at the support. Large shells fabricated off-site must be segmented to be transported before being assembled on-site. The joining mechanism between the shell segments is also key for structural integrity. Both fabrication precision and assembly tolerance are needed to fit the segments together. These joints can potentially lead to new failure modes that reduce the structural integrity of the shells, which should be taken into account. Yet, the necessary segmentation presents the opportunity for deconstruction and reassembly, instead of demolition, thanks to reversible connections, and provides a lightweight assembly process on-site with standard scaffold elements.

This research, part of the UKRI-funded project Automating Concrete Construction (ACORN) [47], has developed a prototype of a segmented concrete shell as a building floor system for circular construction that tackles the challenges previously mentioned. The project aimed to develop such a structural system, including the segmentation and joining, and this paper focuses on the fabrication and assembly process. The main objective is to obtain a drastic reduction in the environmental impact of this floor system, thanks to its structural efficiency, its sustainable buildability, and its potential role in a circular economy of construction.

1.3. Contributions and outline

This paper presents a structurally efficient lightweight concrete shell, fabricated and assembled in a low-waste and low-carbon process, following a design-and-build approach for disassembly and reuse. The realisation of the 4.5m x 4.5m concrete shell, shown in Figure 1 with its support system of ties and columns and its levelled floor, and its sustainability assessment, demonstrate the potential of this prototype, nicknamed the OAK. Section 2 presents the structural system and its design, informed by architectural, engineering, and construction considerations. Section 3 details the digital fabrication of the prototype in the context of off-site automation using a reconfigurable mould and robotic concrete spraying. Section 4 describes the lightweight assembly and disassembly of the prototype on-site using standard scaffold elements, proving the potential for reuse in a circular economy of construction. Section 5 provides a sustainability assessment of the prototype, including the fabrication and assembly process, using life-cycle analysis to assess carbon emission, energy consumption and waste production.

2. Conceptual and structural design

The structural design of the shell, rendered in Figure 2, was informed by construction-related considerations, including building integration, fabrication, transport, assembly and reuse [17].

Figure 2: Render of the shell on columns, with tie-rods countering the thrust, after form finding, segmentation design, and connection detailing, including architectural, engineering, and construction requirements.

Exploration of the shell design was enabled by an automated design framework composed of parametric design tools packaged as a novel plugin called *SQUIRREL*, developed in the scope of ACORN, and implemented in the commercial software Grasshopper3D for Rhino3D [55]. The existing Grasshopper plugins and tools used were Kiwi3D [34] for form finding with isogeometric analysis (IGA) and Karamba3D [52] for structural analysis using Finite Element Analysis (FEA). IGA provides the shape of a monolithic shell, whereas FEA informs the design of the rib and segmentation patterns of this monolithic shell, thanks to stress analysis and topology optimisation. FEA also guides the whole process by assessing the structural behaviour, including buckling, of the segmented ribbed shell. The different load cases shown in Figure 3 were considered to account for the variability of live load patterns that a floor experiences.

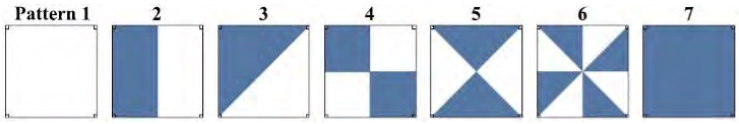

Figure 3: Load application (in blue) following various symmetric and asymmetric loading patterns [26].

2.1. Form finding

The shell had a span of 4.5m, covering a square area of 20m^2. Its shape was defined through form finding using IGA to simulate a membrane structure in compression, using two parameters for surface prestress and edge prestress to vary the final shape. The chamfered square defines the boundary of a planar NURBS surface that is modelled as a membrane structural element, with a surface refinement factor of 15, a default material stiffness of 1GPa, a thickness of 1mm, and a surface stress of 0.335kN/m in both directions. The edges of the surface are converted into cable elements to enable some control of the shape of the shell, with a curve refinement factor of 8, a default material stiffness of 210GPa, a diameter of 10mm, and an edge force of 0.915kN. The resulting shell behaved mainly in compression under a uniform load, which corresponds to the primary load case. The stress distribution in the shell was relatively uniform, except for concentration

along the shallower edges, resulting in a dome-like shape with positive double curvature everywhere. The rise of 59cm in the centre provided a rise-to-span ratio of around 1/8, leading to a shallow geometry to limit height usage. Form-finding parameters were fine-tuned in order to accommodate a 30cm diameter duct running along the edge of the shell, representative of building services that can be integrated within the structural depth. The thickness increased from 3cm at the apex to 6cm at the supports, where compression forces concentrate towards the columns, resulting in an average thickness of 4.5cm, i.e. $1/100^{\text{th}}$ of the span, as opposed to common ratios of around $1/30^{\text{th}}$ for a flat concrete slab. The cross-section in Figure 4 highlights how slender and shallow the shell was while still providing the space needed for services between the structural shell and the functional floor.

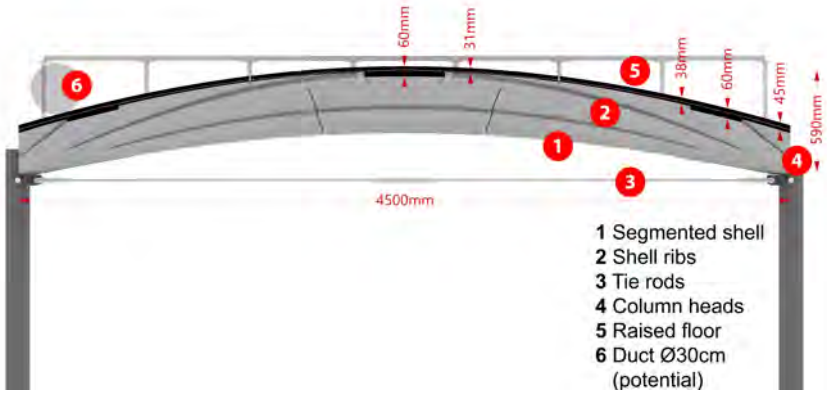

Figure 4: Cross-section of the shell and other building components at mid-span.

A set of ribs stiffened and strengthened the shell, by creating a local thickness of 6cm, like the maximum shell thickness at the supports, across a width of 30cm. The ribs followed the force flow, with two crossing diagonals and arches along the edges between adjacent supports. The pattern of the ribs was also informed by a structural optimisation design process using FEA and Bi-directional Evolutionary Structural Optimisation (BESO) [30] on a monolithic shell for a set of asymmetrical load cases (Figure 5a). The implementation in Karamba3D was used [52]. The parameters were chosen based on a preliminary study exploring their influence [39]. The input parameters were a target mass ratio of 0.24, a maximum number of iterations of 15, a ratio between the maximum number of elements to be added per step and all the elements of 0.02, and a thickness used for softening the shell elements of 1mm. The analysis considered all the symmetrical and asymmetrical load patterns in Figure 3 including the different horizontal rotations and symmetries. The resulting topology optimisation layouts for each load case were added into a combined thickness optimisation layout with a variation of thickness values throughout. The resulting shell weighed 100kg/m^2, around 25% of the mass of a flat slab option, resulting in a lighter floor and less load on the columns throughout the building and on the foundations.

2.2. Segmentation design

The shell was segmented for prefabrication and disassembly. The segments must be smaller than 1.8m x 1.8m, a constraint driven by the size of the mould and the casting area, which was here a stronger constraint than the one due to transportation with a standard lorry with dimensions of around 2m x 4m x 12m. In an industrial context, the segments can be produced on a larger mould of size up to 4m x 12m and still be transported to the site, with proper nesting in the lorry. To simplify fabrication, the interfaces between segments were planar and vertical, instead of being normal to the surface of the shell, so that they could be produced from straight elements that connect into simple nodes. The number of segments was minimised while respecting these size and alignment constraints, resulting in nine segments (Figure 5b).

To prevent in-plane sliding failure, the interfaces between adjacent segments were transverse to the principal compressive stresses, extracted from FEA, which resulted in segmentation joints orthogonal to

the ribs. The central segment had an octagonal shape to maintain the continuity of the diagonal ribs, and the boundary segments were trapezoidal so that the dominant compression forces locked the segments inward. The central segment was the largest with an area of 1.8m x 1.8m and a mass of 300kg. Thanks to symmetry, only three different segment shapes were needed: four identical segments at the corners, four other identical segments on the edge at mid-span, and one at the centre. This repetition was conducive to both prefabrication and reuse.

Table 1 provides the description of the three segment types, including their count, geometry, volume and mass.

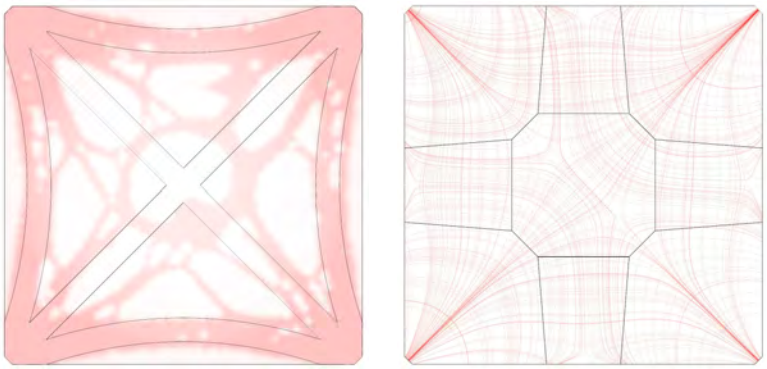

(a) Rib pattern from topology optimisation with BESO.

(b) Shell segmentation from principal stress analysis with FEA.

Figure 5: Design of the shell features (in black) informed by structural analysis and optimisation (in red).

Table 1: Description of the shell segment types.

type	**number**	**shape**	**volume [L]**	**mass [kg]**
edge	4	quadrilateral	60	120
centre	1	octagonal	130	260
corner	4	hexagonal	150	300

2.3. Interface detailing

To enable a circular economy of construction, and thanks to the compression-dominant behaviour of the shell, the joints between the segments were dry – without mortar or grout. Half-joint shear keys along the interfaces guided the assembly process, such as the higher segments being supported by the lower ones, which were eventually supported by columns. They also prevented out-of-plane sliding failure in the direction where the compression forces in the shell induce shear at the interfaces. The keys were interrupted before the extremities of the interfaces, to avoid overlaps, and to provide additional in-plane interlocking between the segments. Figure 6 provides an exploded view of the connections centred on a corner segment and the centre segment.

2.4. Structural analysis

The structural performance of the segmented ribbed shell informed the iterative design process, using FEA to check the maximum deflection, the maximum compression stress, the occurrence of tensile stresses, and the first buckling load factor. Through a mesh convergence analysis, the mesh selected for the structural model has an average edge length of 40mm, corresponding to 90% of the average thickness, accounting for a total of 26k faces. The supports are a set of pinned line boundary conditions along the chamfered edges of the shell, corresponding to the position of the columns, behaving as a stationary hinge that allows rotation around the support line. The load cases included the self-weight G, the additional dead load $G' = 1.0kN/m^2$

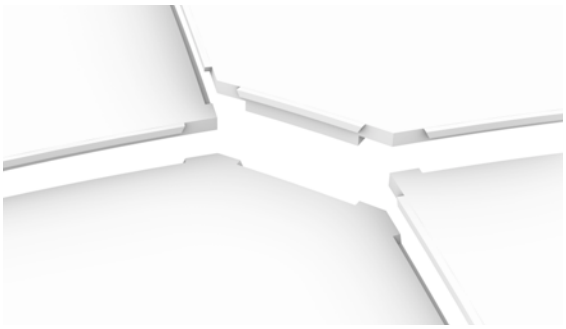

Figure 6: Exploded view of the half-joints acting as shear keys at the interfaces between segments.

and the live load $Q = 1.5kN/m^2$, a low but realistic load for an office programme [15]. The live load case included different symmetric and asymmetric load patterns, shown in Figure 3, similar to [26]. The load combination for the Ultimate Limit State (ULS) was $1.35(G + G') + 1.5Q$ to check strength (stresses) and stability (buckling). For the Serviceability Limit State (SLS), the load combination was $1.0(G + G') + 1.0Q$ to check stiffness (deflection). Though deflection is typically the limiting factor for the serviceability of floors such as flat slabs, it is not critical for compression-dominant structures like shells. The deflection criterion was taken as $1/300^{\text{th}}$ the span of 4.5m $L/300 = 15mm$. The material properties, including admissible stresses of the sprayed fibre-reinforced concrete, are detailed in Section 3. The second-order analysis considered linear elastic material behaviour, a major simplification in the case of concrete and dry-joint interfaces. This compromise was justified by the compression-dominant behaviour of the shell and because it allowed fast interactive design exploration, including form finding and structural analysis. At a later stage, a more accurate structural model would be necessary.

The results of the structural analysis are summarised in Table 2. The structural performance of the final shell design yielded an admissible maximum compression stress of 36MPa at the supports, and a high maximum tensile stress of 17MPa between the ribs, which indicated that the concrete shell would crack and redistribute the stresses on the ribs. The 0.95 quantile values, 3.5MPa for compression and 2.1MPa for tension, highlighted that the maximum stresses were local concentrations and that the stresses were particularly low in the shell, enabling the use of low-strength materials. The first buckling load factor of 9.6, due to a global buckling mode, corresponded to an aimed safety factor of approximately 10. Indeed, buckling is critical for shells in compression, which are particularly sensitive to shape imperfections, especially for shallow shells with a low curvature [54, 40], and this prototype was cast on a flexible formwork, with which imperfections are higher than if cast on a rigid formwork. However, the literature shows that shells with free edges, which have a lower degree of indeterminacy, are less sensitive to imperfections, as they can start buckling, redistribute forces away from these edges, and gain further load capacity [32, 65]. Additionally, geometrical (increase in deformations) and material (low tensile strength) non-linearities were not taken into account in this model, which leads to an overestimate of the buckling resistance, hence aiming for a high safety factor.

These design choices on the shape, the patterns and the joints stemmed from a dialogue in the simultaneous development of the structural system, the off-site fabrication and the on-site assembly processes.

3. Off-site digital fabrication

Off-site manufacturing, automation and robotics were leveraged to develop a fabrication process that results in a low amount of waste, while maintaining high flexibility for the mass-customisation of shell segments for building floors. This section details the mould system and the casting process, and their application to the fabrication of the prototype. This demonstrator was fabricated at the National Research Facility for Infrastructure Sensing (NRFIS) of the Civil Engineering Division at the University of Cambridge.

Table 2: Summary of the structural analysis results using FEA.

	limit state	value	criterion	location	load case
max. deflection [mm]	SLS	6.0	15 (40%)	along boundaries	2
max. compr. stress [MPa]	ULS	36	43 (84%)	near supports	3
.95 quant. compr. stress [MPa]	ULS	3.5	43 (8%)	near supports	3
max. tens. stress [MPa]	ULS	17	9.4 (181%)	between ribs	3
.95 quant. tens. stress [MPa]	ULS	2.1	9.4 (22%)	between ribs	3
first buckling load factor [-]	ULS	9.6	-	global mode	7

3.1. Actuated reconfigurable reusable mould

The low-embodied carbon of concrete shells stemming from their structural efficiency can be compromised by the complexity of fabricating them with a formwork strategy that is wasteful.

To prevent this, the mould system needed the reconfigurability to accommodate the range of shapes that must be created, to be reused without producing waste [50, 46, 20, 57, 37, 35]. Adaptive moulds from Adapa, based on a pin-bed concept, have been used in the industry to produce concrete panels for cladding, or more interestingly for bracing, as in the case of the steel frame of the Kuwait Airport [43]. The workshop of the Department of Engineering at the University of Cambridge produced four 1m x 1m units to create a modular 2m x 2m pin-bed mould shown in Figure 7a, although forming a 4m x 1m mould is also possible to produce shell strips, beams or columns. Each unit has nine vertical actuators arranged in a 3 x 3 grid with 330mm spacing, which are computer controlled. Each actuator can move vertically by up to 400mm and carry a static vertical load of about 25kg, for the production of up to 10cm-thick concrete shells. The concrete is cast once the mould is set in the target configuration through computer control of the actuators.

(a) Overview of the mould

(b) Detail of the flexible formwork

Figure 7: The pin-bed mould consisting of four 1m x 1m modules each with nine actuators supporting and deforming a flexible formwork ©Robin Oval.

The mould was completed by a flexible formwork supported by the grid of actuated pins, as detailed in Figure 7b. This flexible formwork needed to have a balance between flexibility, to safely deform with the movement of pins, and stiffness, to limit the sag between pins, to achieve the range of curvatures needed for the concrete shells. After several design iterations, the flexible formwork consisted of an array of carbon strips spaced by 110mm in the planar configuration. The strips had a cross-section of 12mm x 2mm with a lengthwise tensile modulus of 28-40GPa. The primary strips were the ones directly supported by the pins through 3D-printed (3DP) primary nodes that allowed lateral sliding to reduce transverse forces on the actuators. The secondary strips were the ones supported by the primary ones, thanks to 3DP secondary nodes that also allowed sliding, and rubber bands that kept a regular spacing between successive strips when

the shape configuration changes. The strip network was covered with a textile membrane, commonly used for flexible formwork [25], which was stapled to a timber frame, as shown in Figure 8.

This timber frame delimited the casting area and forms the shear keys by superimposing edges with different profiles. The timber frame edges were all planar and were cut from an 18mm phenolic plywood board with the hand-held CNC router Shaper Origin [59]. The corner nodes of the frame were 3D printed in plastic to align the edges at the required angle. The edges were slid into the node and then held together using screws. Additional metallic strips were attached to the timber edges to stiffen the frame, primarily against the prestress of the textile membrane and the additional pull from the weight of the concrete. The metallic strip are made of flat strips that are fixed perpendicularly to the timber edges thanks to screws and L-shaped brackets. All the elements can be disassembled to be reused to produce identical segments.

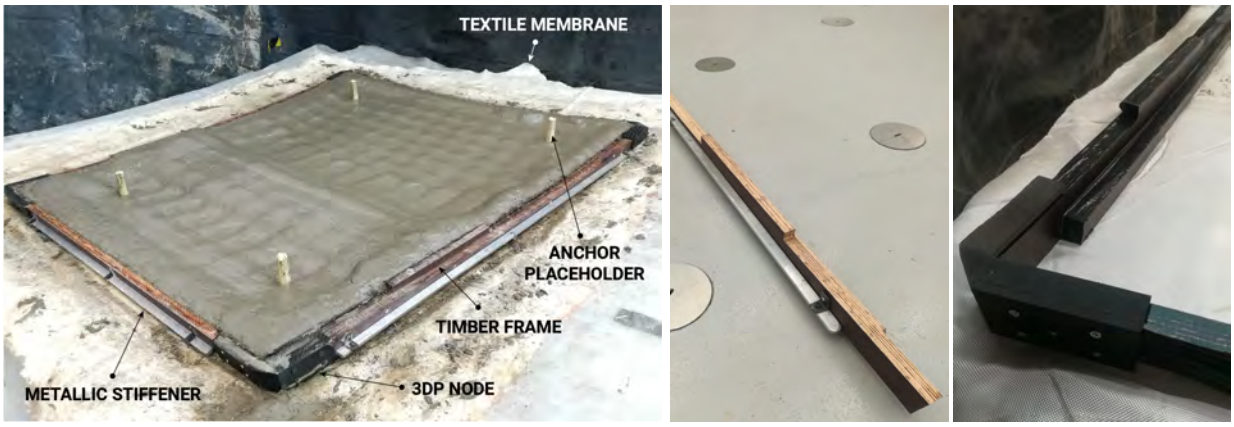

(a) Complete frame after casting (b) Beams (c) Nodes

Figure 8: The reusable frame system as casting area on the flexible mould ©Robin Oval.

The segment was centred on the mould and laid as flat as possible, both maximising the used area of the mould and reducing the risk of slumping on high slopes. This position was automatically found by computing the minimum bounding box of the segment and aligning its local frame with the mould on the digital model. The digital positioning of each segment on the reconfigurable mould also served to check the segmentation during computational design. The base dimension of the bounding box should be smaller than the working area of the mould. Though the frame of the mould modules is 2.0m x 2.0m, the working area was 1.8m x 1.8m as the extreme part of the strips cantilevering from the pins were too flexible to be used to accurately form the shell surface. The depth of the bounding box, i.e. the maximum difference between the pin heights to produce the segment, could not exceed the maximum travel distance of 400mm allowed by the actuators. The frame was manually installed on the mould, guided by the robotic arm that marked the position of the corners of the frame, ready for casting.

3.2. Automated robotic concrete spraying

The flexibility of robotic spraying allows the production of curved shapes [36, 24, 63]. To optimise material distribution, the shell had a variable thickness, from 3cm to 6cm, and thickening ribs for a total thickness of 6cm. An automated digital process allows the accurate deposition of concrete according to the design. Moreover, spraying provides crucial compaction that increases the quality and strength of the structural component. This could not be achieved by vibrating the concrete after pouring without changing the thickness distribution on the sloped surface. Therefore, the shell segments were cast using an automated robotic concrete spraying process [44, 45] shown in Figure 9. A robotic arm, an ABB IRB 6400R, with a reach of 2.8m and a payload of 200kg, carried the spray gun of a PS9000i spray station for glass-fibre reinforced concrete by Power-Sprays. The robotic arm held the spray gun thanks to a 3DP custom gripper combined with a steel mount.

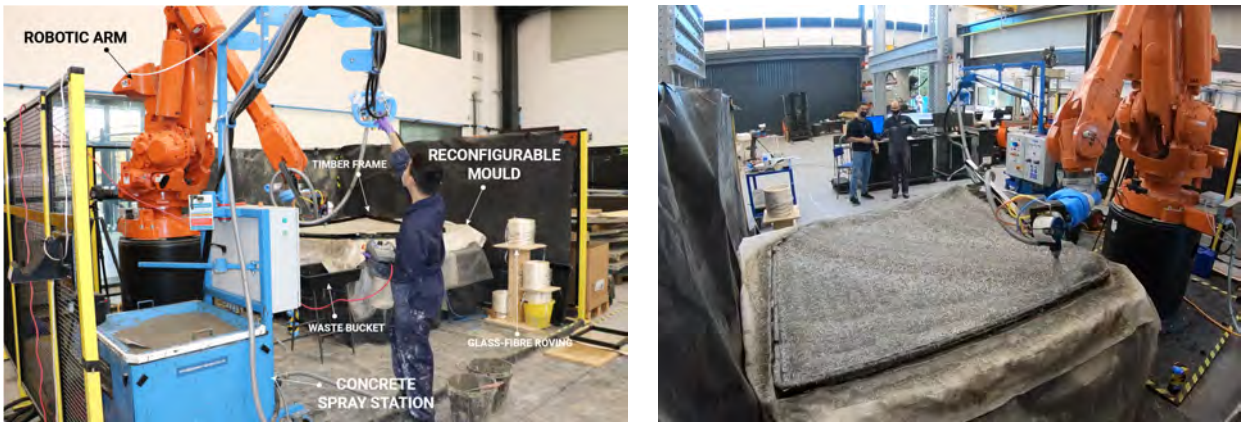

(a) Set-up ©Omar Abo Madyan

(b) Process ©Robin Oval

Figure 9: Automated robotic concrete spraying of ribbed shell segments with double curvature and variable thickness.

3.2.1. Concrete material

Mix design. The fibre reinforcement provided some tensile strength and a ductile behaviour for a material that would otherwise be brittle. The concrete slurry was pumped from the station tank to the spray gun while the fibre was fed separately to the spray gun as a continuous glass filament that was chopped just before spraying, at a chosen length of 25mm. The concrete mix described in Table 3 followed the supplier's recommendation, with kiln-dried sand of grain diameters below 1.0mm for sprayability and additives from Fibre Technologies International Ltd to achieve the desired flowability, pumpability, and curing properties. The cement-sand ratio c/s was 1.0, whereas the water-cement ratio w/c was about 0.28. The quantity of water was tuned while mixing to have a mortar slump test between 3 and 4 as per BS EN 1170-1:1998 [60]. This corresponds to a final diameter between 120mm and 140mm for an initial cylinder with a height of 55mm and a diameter of 55mm, as per the slump test apparatus defined by the standard.

Table 3: Material mix quantities for $1m^3$ of concrete

material	**per m^3**
kiln-dried sand	795kg
CEM II cement	795kg
water	223L
Acrylic Polymer Polycure FT	80L
Super Plasticizer Flowaid FT	4L
Pumping Aid Pumpaid FT	4L
High Zirconia Alkali Resistant Glass Fibre NEG ARG FIBRE AR2500H103 25mm long	100kg

Mechanical properties. The evaluation of the mechanical properties of the sprayed concrete mix stemmed from four compression tests on 40mm cubes and two bending tests on 325mm x 50mm x 40mm prisms per shell segment, the latter as per BS EN 1170-5:1998. These tests were first carried out on a first set after 28 days and then on a second set on the same day as the structural test of the shell. Each set had 36 specimens to test in compression and 18 to test in bending. The average and standard deviation values are shown in Table 4 and Figure 10 shows the specimens after failure.

The concrete had a density of $2.0t/m^3$, typical of a mortar without large aggregate. The mechanical properties increased by about 20% between the two tests, at 28 days and at 12 to 17 weeks, depending on the segment. The compressive strength f_c was similar to a C45/55 with a lower compressive stiffness

Table 4: Concrete mechanical properties

	after 28 days		on test day	
	avrg.	st. dev.	avrg.	st. dev.
f_c [MPa]	42.9	7.1	51.1	7.1
$f_{t,lop}$ [MPa]	7.8	1.5	9.3	1.6
$f_{t,mor}$ [MPa]	9.4	2.3	11.0	2.4
E_{comp} [GPa]	19.9	6.0	26.7	7.8
E_{bend} [GPa]	8.9	1.9	12.9	2.4

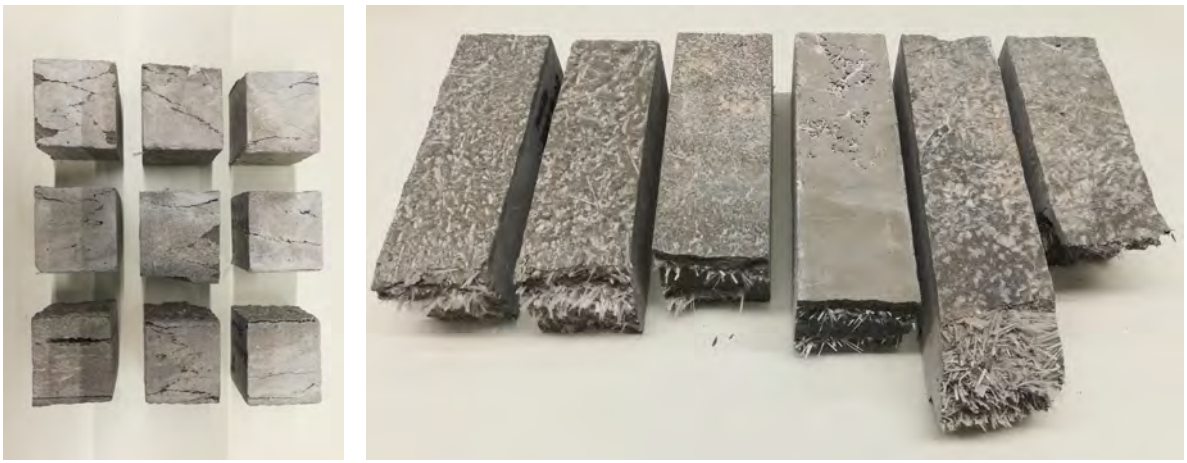

(a) Compression failure

(b) Bending failure

Figure 10: The material tests on small fibre-reinforced concrete specimens ©Mishael Nuh.

E_{comp} from the lack of large aggregates. However, the tensile strength $f_{t,lop}$ when cracks first appear and the tensile strength $f_{t,mor}$ at failure were significantly higher, thanks to the fibre reinforcement. Washout tests at the end of the spray session, consisting of collecting some of the concrete waste, weighing it, washing it to extract the fibres and drying them, provided an actual fibre content ranging between 4% and 11% by weight. The variability in properties derives from casting the segments on different days from different batches, while also improving the production process, which would be reduced in an industrial set-up.

3.2.2. Robotic trajectory

The six degrees of freedom of the robotic arm allow the position and the orientation of the spray gun to be controlled. The reach envelope ranged between 0.8m and 2.8m, which was further reduced with orientation constraints. To resolve reach problems, the shell segments were cast in a convex position, which was the reverse of their final position once assembled, reducing the amount of movement needed by the robot, particularly for high curvatures. This convex position also matched the sag of the fabric between the carbon strips of the formwork with the curvature of the shell segment, close to a physical funicular form-finding process.

The orientation of the spray gun to the sprayed surface was 90° to get a circular spray, and the distance was constant at 225mm, resulting in a spray circle with a diameter of 120mm, since the truncated cone had an angle of 30°. The distance between adjacent passes was set to 40% of the spray circle diameter to create an overlap, resulting in a more uniform deposition. The spray output was set to 12kg/min, or 100cm^3/s. The spray speed across the surface was fixed at 350mm/s, so that each pass of the robot added a layer with a thickness of around 4mm when spraying strips according to Equation 2:

$$t = \frac{V}{A} = (1 + 2\alpha)\frac{Q}{SD} \tag{1}$$

where t is the layer thickness, V the volume sprayed, A the area sprayed, Q the concrete output, S the speed of the spray gun, and D the width of the sprayed strip, which corresponds to the diameter of the sprayed circle, and α the proportion of overlap with the two adjacent passes. Table 5 summarises the main spraying parameters used.

Table 5: Main spraying parameters

parameter	value
spray distance H	225mm
strip width D	120mm
path overlap α	40%
traversal speed S	350mm/s
slurry output Q	12kg/min

Figure 11 summarises the generation of the robotic trajectory. The shell segment was sliced using the bottom surface in contact with the formwork, offset by multiples of the layer thickness, to compute the number of passes per region. As such, the robot sprayed the entire surface first and gradually reduced the area sprayed when some regions have had the required number of passes. To control the material deposition of each layer, the spray passes were offset by a constant distance from each other. On the doubly curved surface, isolines of geodesic curves provided this constant spacing [2]. To reduce the anisotropy of fibre deposition, the spraying passes of the successive layers alternated between multiple directions. The bulk of the segment was sprayed first and the ribs last. The first and last two layers were sprayed without fibres to provide a complete coating of the previous fibres to bond them with the concrete, and to achieve a surface finish without visible fibres. The geometrical operations on the NURBS objects for slicing the volume, computing the geodesic curves and creating the spray trajectory were done in the parametric design environment Grasshopper3D [55], and the inverse kinematics to compute the robotic motions with HAL Robotics [21]. More details on the planning of the robotic trajectory can be found in [45].

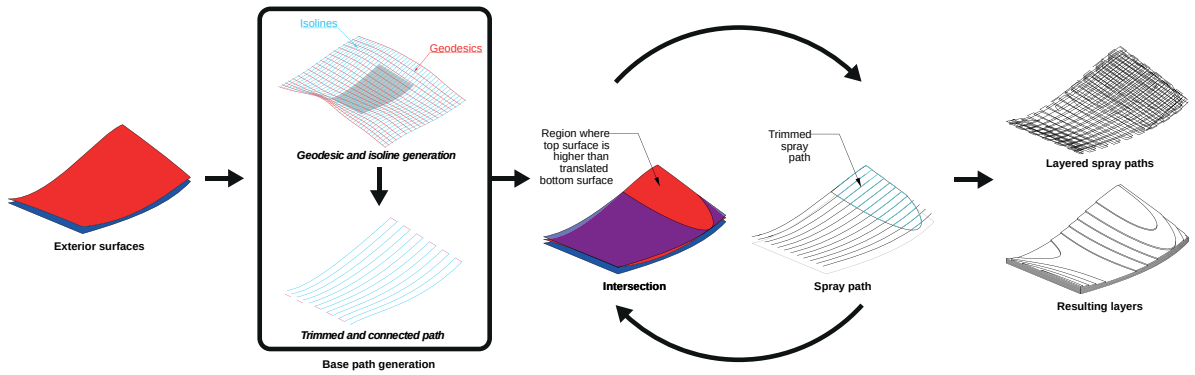

Figure 11: Generation of the trajectory for automated robotic concrete spraying based on computing a network of isolines to the geodesic curves and slicing the shell with variable thickness.

3.3. Results and discussion

This fabrication process had been developed through several preliminary tests and then refined throughout the production of the OAK prototype.

Productivity. Three tests and the final nine segments were cast over eight weeks, including three casts the last week only, once the mixing-spraying-demoulding process had been mastered. Automated spraying enabled a fast casting process with an output of 100cm^3/s. Consequently, spraying a corner segment of 300kg took about 25min. This compares more favourably than other digital fabrication approaches like 3D printing with values between 0.3cm^3/s and 25cm^3/s [8].

Properly filling the concavities necessary to form the male part of the half-joint shear keys proved difficult to automate, even when spraying at an angle. Therefore, these keys, which represented 0.5% of the total volume only, were manually filled before the start of the spraying process.

After casting, a segment was left to cure overnight before demoulding the next day: removing the membrane, lifting the segment, disassembling the frame, and cleaning the different parts for reuse. The segment was lifted using a gantry crane and straps. Lifting was achieved via eye bolts connected through holes formed by cylinders inserted at the end of the casting process. If the reach of the robot was increased thanks to a gantry system, and the flexible formwork of strips was made denser to further reduce the sagging of the fabric, the shell segments could be cast in a convex position to avoid the need to flip them.

Reliability. The spraying process was robust enough to allow pausing to refill the tank of the spray station with concrete, connect or disconnect the filament and the spray gun, change the filament roving, or interrupt the process due to unforeseen incidents, like restarting the air compressor, unblocking the filament, etc. The spray process started and finished at a waste bucket, to which the robot went back every couple of passes, roughly every 5min, to deal with material renewal. Reasonable manual adjustments could occur before spraying the last layers, to fix potential problems like excess material due to the robot looping back to the bucket or to improve the quality of crucial regions like the boundaries.

Waste. Rebound due to the spray process was minimal since the concrete was sprayed downward at a close distance. The material waste mainly came from the passes along the boundary, including some excess material over the timber frame, and the loops back to the waste bucket, which could be eliminated by digitally turning on-and-off spraying. For the last 300kg segment, about 15kg of the sprayed slurry was collected from rebound and over-spray, about 5% of the used volume (see Table 7 in the Appendix). All these material losses could be reduced by scaling up the size of the shell segment and further improving the fabrication process in a factory environment.

Accuracy. A 3mm rubber neoprene was added to the interface to distribute stresses at the concrete-concrete interface and accommodate small surface discrepancies. The first assembly test however showed that these discrepancies were significant. These were due to the flexibility of the casting frame, particularly at the nodes, which did not guarantee the required precision of a couple of millimetres. The 3D-printed plastic nodes did not have the sufficient stiffness to prevent the polygonal frames from shearing deformations. The bending of the timber beams of the frames under the pull of the fabric membrane once the concrete was cast was limited thanks to the stiffening metallic elements along these timber beams. Improvement of the stiffness of the frame through reusable steel elements should increase precision. Particularly, a shell segmentation with a high level of modularity would result in a reasonable number of custom segments, which would justify the use of such expensive moulds. Alternatively, robotic post-processing to mill the edges could guarantee millimetre precision [7], as well as allow more freedom in the shape of the joints. The discrepancy was here solved by grinding and/or adding grout to match the adjacent segments while keeping dry joints. Indeed, at each interface, the lower segment was protected with a plastic sheet during grouting to still allow disassembly after curing and keep a segmented structural system.

Figure 12 shows the scan of the shell using an Artec3D Leo handheld scanner. The intrados exhibited the ribs and the spray pattern, whereas the extrados featured the imprint of the fabric and the strip network of the flexible formwork. The scan was post-processed using registration, cleaning, fusion, hole filling, and isotropic remeshing to obtain a regular mesh to better analyse the thickness distribution.

Thanks to the scans, the accuracy of the normal thickness of the shell could be assessed (Figure 13). At each point i of the scanned mesh, the local thickness t_i was compared with the target thickness t_i^0, after slicing for spraying. The difference was normalised by the maximum target thickness t_{max}^0 of 60mm. The local deviations vary from +100% (60mm) to -25% (-15mm). To estimate a global deviation, the histogram in Figure 14 plots the area-normalised deviation distribution $\bar{t}$, with each mesh sampling point, weighted by their area contribution A_i against the total area A:

$$\bar{t_i} = \frac{A_i}{A} \frac{t_i - t_i^0}{t_{max}^0}. \tag{2}$$

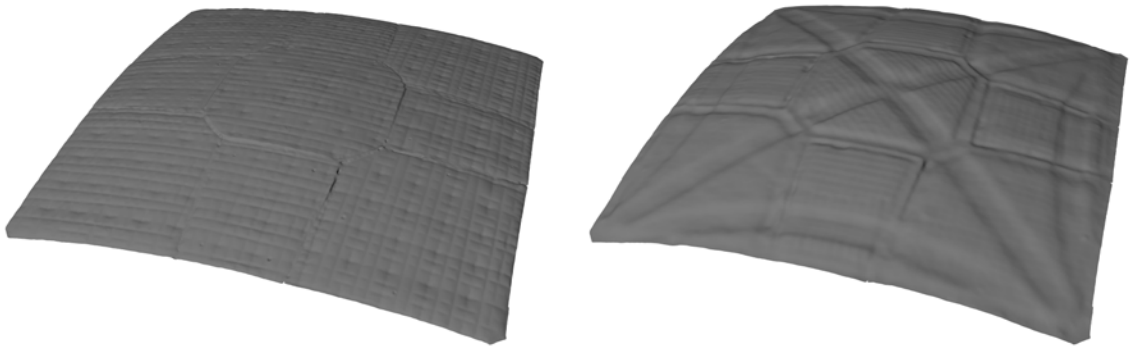

(a) Extrados with formwork imprint (b) Intrados with spray imprint

Figure 12: Post-processed 3D scan of the surfaces of the OAK demonstrator.

This data provided a normalised average of 0.195 (11.7mm), showing that the shell was on average thicker than the target, and a normalised standard deviation of 0.202 (12.1mm), which proved a limited deviation overall. The main deviations occur in two areas: along the boundary of each segment, due to the spray passes that were added after design to strengthen the critical region of the interfaces with their half-joint shear keys; and the shell corners, due to the convergence of the ribs, which required connecting passes that reorient the spraying process between the actual passes over the different ribs. Overall, these results showed good geometrical precision for this prototype. Further details about path planning, geometrical precision, and future improvements can be found in [45].

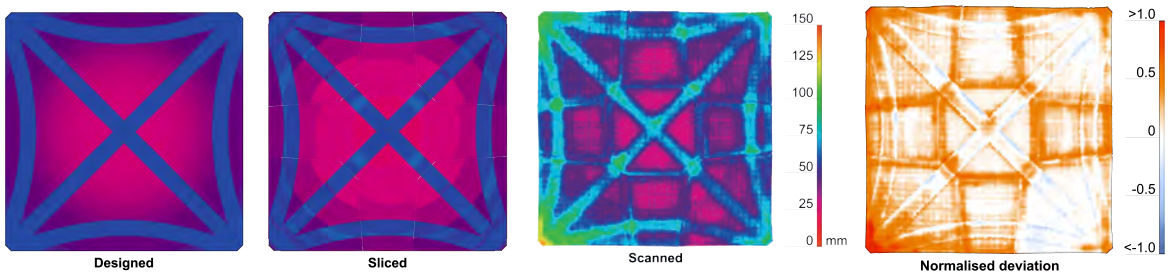

Figure 13: Analysis of the thickness distribution and comparison between the designed shell, the sliced shell in discrete layers for robotic concrete spraying, and the as-built OAK demonstrator.

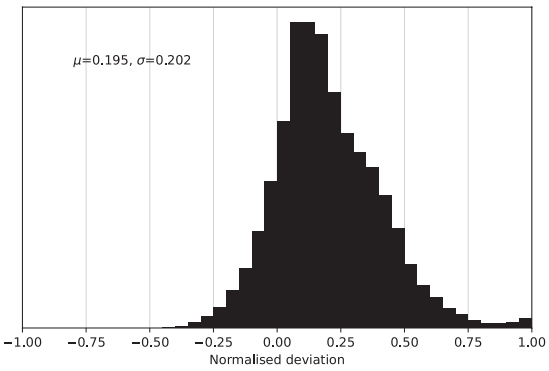

Figure 14: Histogram of the normalised deviation of the local shell thickness weighted by the area contribution of the mesh sampling points.

Material. As the segments were cast on different days, the material quantities and the physical and mechanical properties fluctuate, particularly the fibre ratio and the slurry slump, as shown in Table 7 in the Appendix. A factory context of material batching and quality control would help reduce this variability.

4. On-site lightweight assembly

The shell was prefabricated off-site in large segments that are stacked for transportation and could be assembled on-site. The on-site assembly process should be as simple as possible, using standard construction elements, to reduce waste, time and costs.

4.1. Building integration

The OAK prototype was assembled at the University of Cambridge, integrating the concrete shell with other building components: steel columns, steel tie-rods to counter-act the horizontal thrust, and a raised floor for accessibility, below which building services could be integrated, as shown in Figure 15.

Figure 15: Shell standing once assembled on columns with a levelled floor ©John Orr.

The shell was supported on four tubular columns, made of 2.50m-long hot-formed CHS 139.7/10 in S355 steel. The foot of the column was welded to a base plate bolted to the floor. The connection at the head of the column consisted of welded steel plates to support the shell on a bearing plate, vertical stiffening plates, and anchor plates for the ties. The tie-rods, which balanced the thrust of the shell, are M20 S520 stainless steel tie-bars with mid-span turnbuckles to adjust their length. The levelled floor was an industrial system consisting of tiles and feet with adjustable lengths and a swivel base. This floor simply rested on the shell, creating space suitable for the insertion of ducts and cables for building services.

4.2. Assembly strategy

After an initial assembly and fitting test of the shell on short supports, the process was repeated at height on columns, with some of the key steps illustrated in Figure 16.

Method. The segments were added one at a time. The lower segments rested on the columns and scaffold props, whereas the higher segments rested on the lower ones thanks to the half-joint keys, and scaffold props too for safety. The temporary scaffold props from standard concrete casting formwork were telescopic and used to position the shell segments initially higher than the target, before lowering them into their final position. Once all the joints were closed, the temporary props no longer supported the shell segments and membrane action was activated. For access, several scaffold towers were positioned around the shell, though adjacent floors could be used in the case of a multi-bay building. For safety, a set of formwork props and beams were placed below the shell to prevent the fall of segments in case of collapse, but do not support the shell.

(a) Prefabricated segments ©Robin Oval

(b) Positioning of corner segment ©Pieter Desnerck

(c) Completion of first arch ©Mishael Nuh

(d) Closing of outer ring ©Robin Oval

Figure 16: Assembly of the segmented concrete shell using a set of telescopic formwork props and scaffold towers for access and safety.

Sequence. As equilibrium of the shell segments was crucial, the assembly sequence shown in Figure 17 provided stability at each step, via self-stable elements like arches and a ring. Therefore, the process started by first assembling three segments to form the arch on an edge, then adding the other segments to complete the outer ring arch-by-arch, and finally closing the shell with the central segment. The segments were lifted with the same method as was used for removing them from the mould: using eye bolts and plates running through holes in the segments, acting as anchors for straps connected to a crane.

Decentering. Once all the segments had been installed, the props were iteratively lowered. Before achieving shell action, the segments worked in bending, spanning between the columns and props. The columns initially moved inward because of the offset of the bearing plate from the column axis. Indeed, the tie-rods prevented outward displacement of the columns, but they had the flexibility to move inward by compressing

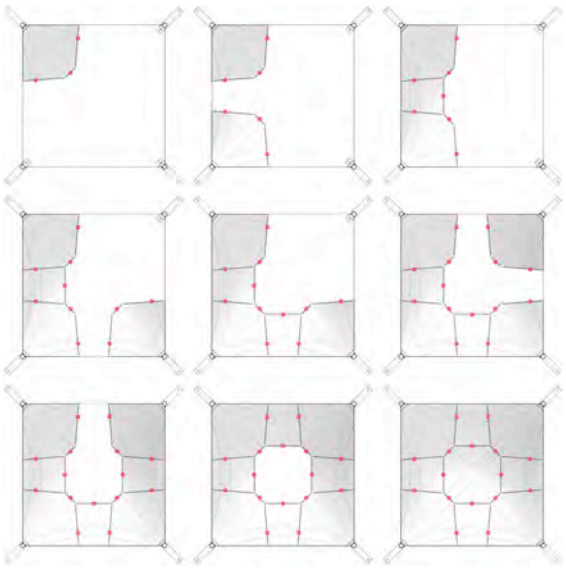

Figure 17: Assembly sequence of the segmented concrete shell by forming intermediary arches and rings to increase stability, with temporary props shown in red.

the tie-rods that then buckle. Then, while lowering the supports, closing the joints, and carrying the loads from bending behaviour to membrane behaviour, the columns gradually moved outward because of the thrust of the shell and by extending the length of the tie-rods using their mid-span turnbuckle. Once the lengths of the tie-rods matched the target span and the columns were vertical, only the height of the temporary props was modified until the shell stood only on the corner columns and the boundary tie-rods.

Disassembly. To disassemble the shell to potentially reuse the segments at the end-of-life of the building, the procedure was simply the reverse of the assembly process. The telescopic props were added back and their height increased by about 50mm to open the joints, shifting back from the membrane behaviour of the shell to the bending behaviour of the independent segments. The segments were then lifted off one by one with a crane, following the reversed assembly sequence, starting with the central segment. This demonstrator was assembled three times: once for an assembly test on short columns, once for showcasing on tall columns, and again for a structural test on short supports, which falls outside the scope of this paper.

5. Cradle-to-gate carbon impact

To evaluate the embodied carbon of this prototype, a life-cycle analysis to estimate its embodied carbon was performed.

5.1. Approach

This study limits the carbon analysis to cradle-to-gate (A1-A3) [61]. The aspects covered for the carbon and energy assessment are the concrete mix, potential transport, fabrication process (materials, formwork, waste, electricity consumption, etc.), tie-rods, and levelled floor. A functional unit of $1m^2$ is the most suitable for this analysis. The project inventory for $1m^2$ is captured from the construction process at the University of Cambridge. The ecoinvent database [19] is used for all background information and inputs and OpenLCA [10] for the calculations and analysis. The transport distance of the raw materials to the factory (A2) is assumed to be 50km. Table 6 details the material quantities and the resulting carbon emissions. The methodology is identical to [14], from which other slab systems are used for benchmarking.

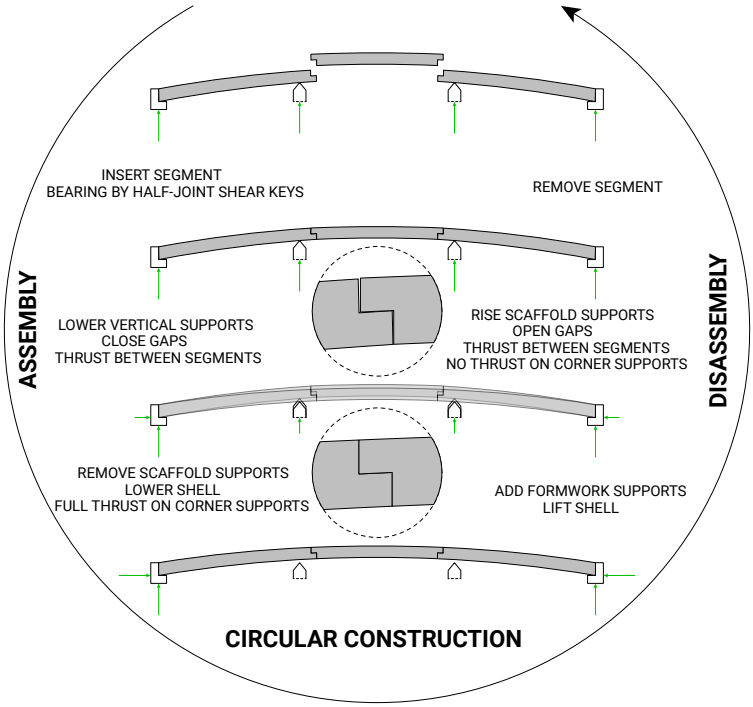

Figure 18: Circular assembly, disassembly, and reuse of a segmented concrete shell using telescopic formwork props thanks to dry half-joint connections.

Table 6: Input quantities and resulting carbon emissions breakdown

stages	**input**	**quantity**	**carbon emissions [kgCO_2eq]**	**comments**
A1	concrete mix	100kg	38.90	no waste considered during batching
	flooring system	29kg	15.50	-
A2	transport of raw materials	50km	3.27	materials locally sourced and delivered to Cambridge
A3	tie rods	4.2kg	16.54	connections not considered
	textile membrane	3.5kg	8.01	full material composition not disclosed by manufacturer
	mould	0.05kg	3.76	only one mould frame made per plywood board
	concrete waste	5kg	1.95	spray splash considered negligible
	electricity consumption	3.2kWh	0.98	concrete mixer and air compressor not included
	total		**88.3**	

5.2. Results

The shell itself is responsible for 72.8kgCO_2eq/m^2, with an additional 15.5kgCO_2eq/m^2 from the levelled floor system (Figure 19). The raw materials (A1) are responsible for most of the emissions, mainly due to

the high cement content in the concrete mix design (Table 3). Then follows the impact of the glass fibre reinforcement and the stainless tie rods. Future work should focus on optimising the concrete mix design and on the glass fibre density distribution. Material transport (A2) is responsible for less than 5% of the carbon emissions. The emissions from the manufacturing stage (A3) are mainly attributed to consumables such as the casting frame, the textile membrane and electricity consumption. The electricity consumption accounts for 4% of emissions, used for the pin-bed mould, the robotic arm, and the spray station. The estimated concrete waste of 5% primarily comes from spray rebound and additional passes over the boundary frame and to the discharge bucket.

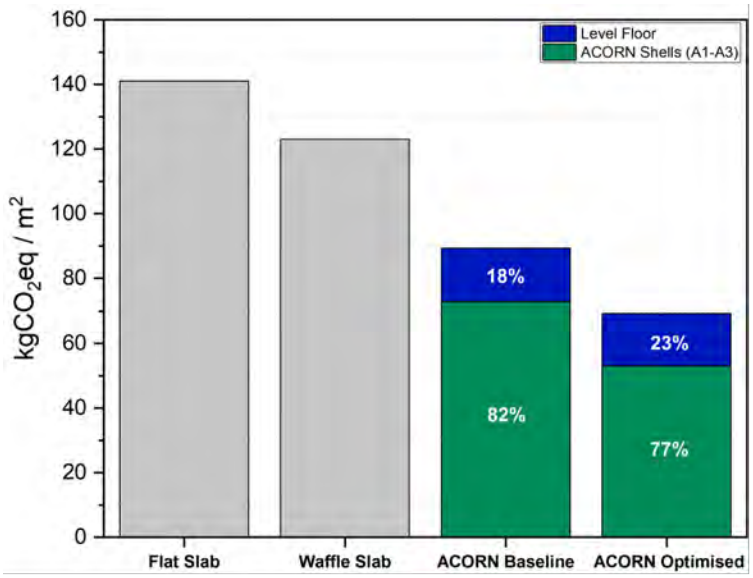

Figure 19: Embodied carbon of concrete floor systems per m^2 of covered plan area

The OAK prototype is compared against two standard concrete floor systems, designed for the same load-bearing capacity: a 250mm-thick flat reinforced slab and a waffle slab with 150mm-deep ribs and a 900mm spacing, both with a C32/40 concrete [14], see results in Figure 19. The depth of the slab and the density of the reinforcement were taken from [22]. The OAK has a 48% lower embodied carbon than the regular flat slab. The levelled floor system is included within the system boundaries for the shell, which increases the embodied carbon by 18%, though the flat and waffle slabs do not have any floor systems or finishes.

Further significant carbon saving can be achieved by transitioning into a more efficient industrialised process. By optimising the following variables, a reduction of 27% from the baseline is possible:

1. Decreasing the diameter of the steel rods from 29mm to 18mm;
2. Substituting 40% of cement by ground-granulated blast-furnace slag (GGBS);
3. Using high-performance and low-wear materials for moulds that can be used up to 100 times, instead of phenolic plywood that was considered to be reusable up to 10 times only;
4. Eliminating waste from overflow and initial dump by adjusting the spraying speed.

These simple procedures and alterations would make it possible to achieve a carbon factor of $53 kgCO_2eq/m^2$ (Figure 19) for ACORN shells. Therefore optimising these parameters can result in a 60% reduction in the concrete shells compared to the embodied carbon of the flat slab. The additional impact of the commercial aluminium levelled floor system, corresponding to 23%, can be reduced by opting for sustainable materials and optimising the fabrication process of the floor. It should also be noted that a conventional slab requires surface finishes and a flooring system as well, which will contribute to the embodied carbon.

Future work will complete the full life-cycle analysis and consider a comprehensive set of sustainability metrics [61]. The remaining stages to evaluate are on-site transport and assembly (A4-A5) and the potential benefits of end-of-life disassembly for reuse (D) in the context of a circular economy of construction.

Thanks to structural efficiency through computational design, digital fabrication, lightweight assembly, and circular construction, ACORN's OAK prototype is a step towards more sustainable building floor systems.

Conclusion

To drastically reduce the environmental impact of the construction industry, we need low-carbon building floors. This paper presented the OAK prototype of the ACORN project, a lightweight concrete shell that allows disassembly for a circular economy of construction. This shell was made of segments that were prefabricated off-site using a low-waste process with a reconfigurable mould and robotic concrete spraying, before being assembled on-site using standard telescopic formwork props. The focus was set on automating the crucial steps, namely moulding and casting, while planning for simplified on-site assembly with reduced falsework. The shell achieved a low carbon footprint per surface area, 60% less than an equivalent flat slab reference, as evidenced by the life-cycle analysis. This achievement was made possible through the shift from plates in bending to shells in compression, and using a holistic approach combining computational design and digital fabrication with a trade-off in the hierarchy of design objectives between structural efficiency and fabrication productivity.

Future work

Future work to improve the sustainability and production of these segmented concrete shells as building floors includes: high-quality casting frames; low-carbon sprayable concrete material; robotic concrete subtractive fabrication for the interlocking connections; topology optimisation of fibre distribution for functionally-graded concrete shells; thinner shell with a deeper network of ribs; inclusion of unbonded post-tensioning for robustness; augmented reality assembly.

As multiple additional requirements come into play for suitable application, future work also needs to consider the following aspects, mainly regarding comfort:

- **Depth use**: the structural depth of a shell is higher than a plate, but may be competitive in terms of floor-to-floor height by integrating building services between the concrete shell and the levelled floor. Moreover, the springing of the shell can start lower than a flat ceiling, the key requirement being the tie-rods remain higher than the doors and windows.
- **Room acoustics**: the concave shape had a point where sound focused. From a geometrical approach, a shallower shell with negative double curvature and deeper ribs can improve the room's acoustic performance as well as the structural performance.
- **Floor insulation**: the segmented nature of the structure, and its permeability to sound, heat, and fire can be resolved by sealing the interfaces and anchor holes with mineral wool for instance, but must remain suitable for disassembly and reuse.
- **Slab vibration**: the low mass m and the high stiffness k of the shell, thanks to its curvature, have the potential to provide a high first natural frequency f to provide a more comfortable response against vibrations, as $f \propto \sqrt{k/m}$.
- **Fire safety**: the thinness of the shell reduces the structural integrity of the concrete against fire, but the compression behaviour with the use of glass fibres instead of steel reinforcement is a benefit of this system. However, the steel tie-rods would need additional protection.

To have an impact on the industry, further research is needed to demonstrate the applicability of such a structure in practice, and answer the questions of comfort, insulation, and fire safety.

CRediT authorship statement

Robin Oval: Conceptualization, Methodology, Software, Investigation, Validation, Writing - original draft, Visualization. **Mishael Nuh**: Methodology, Software, Investigation, Validation, Writing - review & editing, Visualization. **Eduardo Costa**: Conceptualization, Methodology, Software, Formal analysis, Investigation, Writing - original draft, Visualization. **Omar Abo Madyan**: Formal analysis, Investigation, Data Curation, Validation, Writing - original draft, Visualization. **John Orr**: Writing - review & editing, Resources, Supervision, Funding acquisition. **Paul Shepherd**: Writing - review & editing, Supervision, Project administration, Funding acquisition.

Declaration of Competing Interest

The authors declare that they have no known competing financial interests or personal relationships that could have appeared to influence the work reported in this paper.

Acknowledgements

The *Automating Concrete Construction* (ACORN) research project was funded by UKRI through the ISCF Transforming Construction programme, grant number EP/S031316/1. The authors thank the ACORN and NRFIS lab management and technical team: Ricardo Osuna-Perdomo, Diana Thomas-McEwen, Pieter Desnerck, Martin Touhey, Phil McLaren, and Connor Humphreys. The authors also thank the rest of the ACORN team for their support: Saverio Spadea, Daniel Summerbell, Maxime Pollet, Anna Perepechay, Hannah Dennis, Jennifer Schooling, as well as the industrial project partners and affiliates for their feedback.

References

[1] Adapa - Adaptive moulds. Accessed on 17/06/2022.

[2] Emil Adiels, Mats Ander, and Chris JK Williams. Brick patterns on shells using geodesic coordinates. In *Proceedings of IASS Annual Symposium 2017*. International Association for Shell and Spatial Structures (IASS), 2017.

[3] Sigrid Adriaenssens, Philippe Block, Diederik Veenendaal, and Chris Williams. *Shell structures for architecture: form finding and optimization*. Routledge, 2014.

[4] Jane Anderson and Alice Moncaster. Embodied carbon of concrete in buildings, part 1: analysis of published EPD. *Buildings and Cities*, 2020.

[5] BIS. Estimating the amount of CO2 emissions that the construction industry can influence - supporting material for the Low Carbon Construction IGT Report, 2010.

[6] Philippe Block, Cristián Calvo Barentin, Francesco Ranaudo, and Noelle Paulson. Imposing challenges, disruptive changes: rethinking the floor slab. In *The materials book: inspired by the 6th LafargeHolcim Foundation Forum*. Forum Ruby Press Berlin, 2019.

[7] Richard Buswell, Jie Xu, Daniel De Becker, James Dobrzanski, John Provis, John Temitope Kolawole, and Peter Kinnell. Geometric quality assurance for 3d concrete printing and hybrid construction manufacturing using a standardised test part for benchmarking capability. *Cement and Concrete Research*, 156:106773, 2022.

[8] Richard A Buswell, WR Leal De Silva, Scott Z Jones, and Justin Dirrenberger. 3d printing using concrete extrusion: A roadmap for research. *Cement and Concrete Research*, 112:37–49, 2018.

[9] A Churakov. Biaxial hollow slab with innovative types of voids. *Stroitel'stvo Unikal'nyh Zdanij i Sooruzenij*, 2014.

[10] Andreas Ciroth. ICT for environment in life cycle applications openLCA—A new open source software for life cycle assessment. *The international journal of life cycle assessment*, 12(4):209–210, 2007.

[11] C Borg Costanzi, ZY Ahmed, H Roel Schipper, FP Bos, Ulrich Knaack, and RJM Wolfs. 3d printing concrete on temporary surfaces: The design and fabrication of a concrete shell structure. *Automation in Construction*, 94:395–404, 2018.

[12] Pierre Cuvilliers, Cyril Douthe, Lionel du Peloux, and Robert Le Roy. Hybrid structural skin: prototype of a GFRP elastic gridshell braced by a fiber-reinforced concrete envelope. *Journal of the International Association for Shell and Spatial Structures*, 58(1):65–78, 2017.

[13] Borja García de Soto, Isolda Agustí-Juan, Jens Hunhevicz, Samuel Joss, Konrad Graser, Guillaume Habert, and Bryan T Adey. Productivity of digital fabrication in construction: Cost and time analysis of a robotically built wall. *Automation in Construction*, 92:297–311, 2018.

[14] Michal Drewniok. Relationships between building structural parameters and embodied carbon part 1: Early-stage design decisions. Technical report, University of Cambridge, 2021.

[15] Michal Drewniok and John Orr. Minimising energy in construction: Demonstrating floor loading - report meicon minimising energy in construction.

[16] Romain Duballet, Olivier Baverel, and Justin Dirrenberger. Space truss masonry walls with robotic mortar extrusion. *Structures*, 18:41–47, 2019.
[17] Eduardo Castro e Costa, Robin Oval, Paul Shepherd, and John Orr. Fabrication-aware parametric design of segmented concrete shells. In *Proceedings of IASS Annual Symposium 2021*. International Association for Shell and Spatial Structures (IASS), 2021.
[18] Tomás Méndez Echenagucia, Dave Pigram, Andrew Liew, Tom Van Mele, and Philippe Block. A cable-net and fabric formwork system for the construction of concrete shells: design, fabrication and construction of a full scale prototype. *Structures*, 18:72–82, 2019.
[19] ecoinvent - For the availability of environmental data worldwide. Accessed on 31/03/2022.
[20] Pavlos Fereos and Marios Tsiliakos. Isoprototyping-rapid robotic aided fabrication for double curvature surfaces. In *eCAADe 32*. CUMINCAD, 2014.
[21] Tristan Góbin, Sebastian Andraos, Thibault Schwartz, and Rémi Vriet. HAL Robotics Framework. In *Proceedings of the International Symposium on Automation and Robotics in Construction (ISARC)*, volume 38, pages 733–740. IAARC Publications, 2021.
[22] CH Goodchild, RM Webster, and KS Elliott. Economic concrete frame elements to eurocode 2. *The Concrete Centre, Camberley, Surrey, UK*, 2009.
[23] Clément Gosselin, Romain Duballet, Philippe Roux, Nadja Gaudillière, Justin Dirrenberger, and Philippe Morel. Large-scale 3d printing of ultra-high performance concrete–a new processing route for architects and builders. *Materials & Design*, 100:102–109, 2016.
[24] Norman Hack and Harald Kloft. Shotcrete 3d printing technology for the fabrication of slender fully reinforced freeform concrete elements with high surface quality: a real-scale demonstrator. In *Second RILEM International Conference on Concrete and Digital Fabrication*, pages 1128–1137. Springer, 2020.
[25] Will Hawkins, Michael Herrmann, Tim Ibell, Benjamin Kromoser, Alexander Michaelski, John Orr, Remo Pedreschi, Arno Pronk, Roel Schipper, Paul Shepherd, et al. Flexible formwork technologies–a state of the art review. *Structural Concrete*, 17(6):911–935, 2016.
[26] Will Hawkins, John Orr, Paul Shepherd, and Tim Ibell. Design, construction and testing of a low carbon thin-shell concrete flooring system. *Structures*, 2019.
[27] Hans-Dieter Hecker. Der Hörsaal des Zoologischen Instituts der Universität Freiburg. *Freiburger Universitätsblätter*, 25:49–52, 1969.
[28] Jacques Heyman. *Equilibrium of shell structures*. The Oxford Engineering Science Series, 1977.
[29] Holedeck. Accessed on 07/04/2022.
[30] Xiaodong Huang and Mike Xie. *Evolutionary topology optimization of continuum structures: methods and applications*. John Wiley & Sons, 2010.
[31] Gene TC Kao, Axel Körner, Daniel Sonntag, Long Nguyen, Achim Menges, and Jan Knippers. Assembly-aware design of masonry shell structures: a computational approach. In *Proceedings of IASS Annual Symposium 2017*. International Association for Shell and Spatial Structures (IASS), 2017.
[32] Lajos Kollár and E Dulacsha. *Buckling of shells for engineers*. John Wiley & Sons, 1984.
[33] Robert H Lab. Think formwork - reduce costs. *Structure magazine*, 2007.
[34] Philipp Längst, Anna M Bauer, Alexander Michalski, and Julian Lienhard. The potentials of isogeometric analysis methods in integrated design processes. In *Proceedings of IASS Annual Symposium 2017*. International Association for Shell and Spatial Structures (IASS), 2017.
[35] Jian Hui Lim, Yiwei Weng, and Quang-Cuong Pham. 3d printing of curved concrete surfaces using adaptable membrane formwork. *Construction and Building Materials*, 232:117075, 2020.
[36] H Lindemann, R Gerbers, S Ibrahim, F Dietrich, E Herrmann, K Dröder, A Raatz, and H Kloft. Development of a shotcrete 3d-printing (sc3dp) technology for additive manufacturing of reinforced freeform concrete structures. In *First RILEM International Conference on Concrete and Digital Fabrication*, pages 287–298. Springer, 2018.
[37] Paul Loh, David Leggett, and Daniel Prohasky. Cnc adjustable mould to eliminate waste in concrete casting. In *Proceedings of eCAADe 36*. CUMINCAD, 2018.
[38] S Maitenaz, M Charrier, R Mesnil, P Onfroy, N Metge, A Feraille, and JF Caron. Fabrication of a truss-like beam casted with 3d printed clay moulds. In *ISARC. Proceedings of the International Symposium on Automation and Robotics in Construction*, volume 38, pages 712–716. IAARC Publications, 2021.
[39] Sára Mándoki. Automating concrete construction: Development of a topology optimised shell. Technical report, University of Cambridge, 2021.
[40] Stefan J Medwadowski. Buckling of concrete shells: an overview. *Journal of the International Association for Shell and Spatial structures*, 45(1):51–63, 2004.
[41] Mahan Motamedi, Romain Mesnil, Robin Oval, and Olivier Baverel. Scaffold-free 3d printing of shells: Introduction to patching grammar. *Automation in Construction*, 139:104306, 2022.
[42] Pier Luigi Nervi. *Aesthetics and technology in building*. Charles Eliot Norton lectures. Harvard University Press, 1965.
[43] Guido Nieri, Lucio Blandini, and Werner Sobek. Kuwait international airport terminal 2: Detailed design and fabrication of a large-span composite shell. In *Proceedings of IASS Annual Symposium 2019*. International Association for Shell and Spatial Structures (IASS), 2019.
[44] Mishael Nuh, Robin Oval, and John Orr. ARCS: Automated Robotic Concrete Spraying for the fabrication of variable thickness doubly curved shells. In *Third RILEM International Conference on Concrete and Digital Fabrication*. Springer, 2022.
[45] Mishael Nuh, Robin Oval, John Orr, and Paul Shepherd. Digital fabrication of ribbed concrete shells using automated

robotic concrete spraying. *Additive Manufacturing*, page 103159, 2022.
[46] Silvan Oesterle, Axel Vansteenkiste, and Ammar Mirjan. Zero waste free-form formwork. In *Proceedings of the Second International Conference on Flexible Formwork*, pages 258–267. BRE CICM, University of Bath, 2012.
[47] Robin Oval, Eduardo Castro e Costa, Diana Thomas-McEwan, Mishael Nuh, John Orr, and Paul Shepherd. A path towards off-site automated fabrication of segmented concrete shells as building floors. In *Proceedings of IASS Annual Symposium 2021*. International Association for Shell and Spatial Structures (IASS), 2021.
[48] Stefana Parascho, Isla Xi Han, Alessandro Beghini, Masaaki Miki, Samantha Walker, Edvard PG Bruun, and Sigrid Adriaenssens. Lightvault: a design and robotic fabrication method for complex masonry structures. *Advances in Architectural Geometry*, 2021.
[49] Vittorio Paris, Attilio Pizzigoni, and Sigrid Adriaenssens. Statics of self-balancing masonry domes constructed with a cross-herringbone spiraling pattern. *Engineering Structures*, 215:110440, 2020.
[50] Troels H Pedersen and Torben A Lenau. Variable geometry casting of concrete elements using pin-type tooling. *Journal of manufacturing science and engineering*, 132(6), 2010.
[51] Mariana Popescu, Matthias Rippmann, Andrew Liew, Lex Reiter, Robert J Flatt, Tom Van Mele, and Philippe Block. Structural design, digital fabrication and construction of the cable-net and knitted formwork of the knitcandela concrete shell. *Structures*, 31:1287–1299, 2021.
[52] Clemens Preisinger. Linking structure and parametric geometry. *Architectural Design*, 83(2):110–113, 2013.
[53] Francesco Ranaudo, Tom Van Mele, and Philippe Block. A low-carbon, funicular concrete floor system: design and engineering of the hilo floors. *System*, 2012(2016):2016–2018, 2010.
[54] R Reitinger and E Ramm. Buckling and imperfection sensitivity in the optimization of shell structures. *Thin-walled structures*, 23:159–177, 1995.
[55] David Rutten, Robert McNeel, et al. Grasshopper3d. *Robert McNeel & Associates: Seattle, WA, USA*, 2007.
[56] Wasim Salama. Design of concrete buildings for disassembly: An explorative review. *International Journal of Sustainable Built Environment*, 6(2):617–635, 2017.
[57] HR Schipper. *Double-curved precast concrete elements: Research into technical viability of the flexible mould method*. PhD thesis, TU Delft, 2015.
[58] Anand Shah and Shehzad Irani. Design and construction of a novel slab system using bending active framework. In *Proceedings of fib Symposium on Conceptual Design of Structures*. fib, 2019.
[59] Shaper Origin - Precision Cutting Simplified. Accessed on 09/03/2022.
[60] European Standards. BS EN 1170-1:1998 - precast concrete products. test method for glass-fibre reinforced cement measuring the consistency of the matrix. 'slump test' method., 1998. Accessed on 13/06/2022.
[61] European Standards. BS EN 15978:2011 - sustainability of construction works. assessment of environmental performance of buildings. calculation method., 2012. Accessed on 13/06/2022.
[62] Anna Szabo, Patrick Bedarf, and Benjamin Dillenburger. Robotic 3d printing of mineral foam for a lightweight composite concrete slab. In *Proceedings of CAADRIA 27*, volume 2, pages 61–70. CAADRIA, 2022.
[63] Nizar Taha, Alexander N Walzer, Jetana Ruangjun, Theophil Bürgin, Kathrin Dörfler, Ena Lloret-Fritschi, Fabio Gramazio, and Matthias Kohler. Robotic aerocrete–a novel robotic spraying and surface treatment technology for the production of slender reinforced concrete elements. In *Architecture in the Age of the 4th Industrial Revolution–Proceedings of the 37th eCAADe and 23rd SIGraDi Conference*, volume 3, pages 245–254. CumInCAD, 2019.
[64] Gabriel Tang and Remo Pedreschi. Gridshell as formwork: Proof of concept for a new technique for constructing thin concrete shells supported by gridshell as formwork. *Journal of Architectural Engineering*, 26(4):04020036, 2020.
[65] Antonio Tomás and Juan Pedro Tovar. The influence of initial geometric imperfections on the buckling load of single and double curvature concrete shells. *Computers & structures*, 96:34–45, 2012.

Appendix

Table 7: Production data on the fabrication of the shell segments using automated robotic concrete spraying

Date	**Type**	**Concrete mix**						**Sprayer settings**				**Material test results**				**Waste**
		Cement [kg]	Sand [kg]	Polycure [L]	Flowaid [mL]	Pumpaid [mL]	Water [L]	Air mover [psi]	Spray air [psi]	Chopper motor [psi]	Motor [rpm]	Fibre bag test [g/15s]	Slurry bucket test [kg/30s]	Slurry slump test [rings]	Wash-out test fibre ratio [-]	Sprayed concrete [kg]
10/21/21	Edge	100	100	10	500	500	29	25	35	30	92	146	6	4	-	24
10/26/21	Edge	100	100	10	500	500	25.8	25	35	34	99	163	6.1	3	4.10%	-
10/28/21	Edge	100	100	10	500	500	24.4	25	35	35	104	159	5.9	3	7.70%	-
11/02/21	Edge	100	100	10	500	500	25.5	25	35	35	103	160	6.1	3	5.00%	-
11/05/21	Centre	250	250	25	1250	1250	67.4	25	35	32	103	160	6.3	3	9.70%	-
11/11/21	Corner	200	200	20	1000	1000	52.5	30	35	30	99	156	6.1	4 /4	8.60%	17
11/15/21	Corner	200	200	20	1000	1000	51.8	30	35	30	93	148	6.1	3.5 / 4	7.70%	24
11/17/21	Corner	200	200	20	1000	1000	51.4	30	35	30	93	163	6	3 / 3.5	11.60%	16
11/19/21	Corner	200	200	20	1000	1000	50.5	30	35	30	93	158	6.1	4 / 3	9.50%	15